Catalysis Today 147S (2009) S237–S243

Contents lists available at ScienceDirect

Catalysis Today

journal homepage: www.elsevier.com/locate/cattod

Structured catalyst and combined reactor loading for methane combustion in a gas turbine power plant

Svetlana A. Yashnik [a], Nadezhda V. Shikina [a], Zinfer R. Ismagilov [a,*], Andrei N. Zagoruiko [a], Mikhail A. Kerzhentsev [a], Valentin N. Parmon [a], Vladimir M. Zakharov [b], Boris I. Braynin [b], Oleg N. Favorski [b], Askhat M. Gumerov [c]

[a] Boreskov Institute of Catalysis, Novosibirsk, Russia
[b] Central Institute of Aviation Motors, Moscow, Russia
[c] Kazan Technical University, Kazan, Russia

ARTICLE INFO

Article history:
Available online 5 August 2009

Keywords:
Methane catalytic combustion
Gas turbine power plant
Pd-ceria catalyst
Pd-hexaaluminate catalyst

ABSTRACT

Modeling of methane combustion in several types of catalyst packages composed of 2 or 3 beds of granulated catalysts with different chemical compositions, shapes and sizes of pellets has been performed. It has been shown that the high efficiency of methane combustion (>99.97%) and low emission of HC < 10 ppm can be achieved for all types of catalyst packages at variation of the inlet temperature. Experimental runs in a model reactor (1.3 kg catalyst) have demonstrated very good correlation with the results of the modeling.

1. Introduction

The central problem of power generation is environmental safety, and first of all, the reduction of the emission of toxic substances (NO_x, CO, hydrocarbons) as well as greenhouse gases (CO_2 and H_2O). The use of heterogeneous catalytic oxidation of natural gas and hydrocarbon fuels makes possible a substantial temperature decrease in the burning zone, hence the thermal NO_x formation is practically completely excluded [1–6]. The utilization of lean fuel–air mixtures permits essential reduction of the emissions of carbon dioxide and water vapor [5].

Ultra-low emission operation parameters can be achieved by using catalyst in combustion chambers of gas turbines. The catalyst in a gas-turbine combustor has to withstand continuous operation for at least 10,000 h under severe operation conditions: high gas hourly space velocity (GHSV) and temperatures over 1200 K [7]. Material development is therefore one of the key issues in the development of catalytic combustion for gas turbines. Such catalyst has to possess high mechanical strength and the ability to initiate methane oxidation in lean mixtures at low temperatures and maintain stable oxidation during long time at temperatures above 1200 K [3,6].

At present, methane combustion in gas turbines mostly proceeds over a uniform structured catalytic package consisting of monolithic catalysts prepared by deposition of porous washcoat and catalytically active component (usually 5 wt.% Pd) on a metal monolith [3,8–10].

Catalytic combustion chamber with a granulated catalyst is another option for low power turbines [11–13]. Earlier we have developed a granulated oxide catalyst Mn-La-Al_2O_3 [14,15] and palladium catalysts Pd-CeO_2-Al_2O_3 [12,16] and Pd-Mn-La-Al_2O_3 [15] with a low Pd content for high temperature oxidation of lean methane–air mixtures. It is important to note that the active component phases in the catalysts are formed at high temperatures 1173–1273 K, and so these catalysts have high thermal stability and can be used in catalytic combustion chambers (CCCs) of power turbines. Successful development of the CCC with granular catalysts requires the optimization of the catalyst bed activity and high temperature stability [12,13] simultaneously with minimization of the pressure drop, which can be performed by variation of the shape and size of granules, as well as by variation of the structure of a combined catalyst packing in the reactor.

In this paper we present results of modeling and experimental study of three types of structured loadings of the reactor: variation of catalytic activity with shape of granules for a uniform loading and combined loadings consisting of two or three different catalysts.

2. Experimental

2.1. Catalyst preparation

Pilot batches of the following catalysts: Pd-Ce-Al_2O_3 (commercial trademark IC-12-60), Mn-La-Al_2O_3 (IC-12-61), and Pd-Mn-La-

* Corresponding author.
E-mail address: zri@catalysis.ru (Z.R. Ismagilov).

0920-5861/$ – see front matter © 2009 Elsevier B.V. All rights reserved.
doi:10.1016/j.cattod.2009.07.042

Table 1
Physico-chemical and catalytic properties of Pd-CeO_2-Al_2O_3, Pd-Mn-hexaaluminate, and Mn-hexaaluminate catalysts.

No.	Catalyst	Chemical composition by		Physical properties			Catalytic properties				
		Spectral X-ray fluorescence analysis (wt.%)	X-ray diffraction	S_{sp} (m^2/g)	V_Σ (cm^3/g)	P_c (kg/cm^2)	T_{ign} (K)	CH_4, CO, NO_x outlet concentrations at T_{in}			
								T_{in} (K)	CH_4 (ppm)	CO (ppm)	NO_x (ppm)
1	IC-12-61	Mn−6.9, La−10.1	$MnLaAl_{11}O_{19}$, $LaAlO_3$, $\gamma^{\#}$-Al_2O_3	43	0.18	34	640	836	135	33	1
2	IC-12-60/1	Pd−2.1, Ce−10.1	δ-Al_2O_3, CeO_2 ($D \sim 210$ Å) PdO ($D \sim 400$ Å)	53	0.37	22	575	827	63	18	0
3	IC-12-60/2	Pd−2.1, Ce−10.1	δ-Al_2O_3, CeO_2 ($D \sim 200$ Å), PdO ($D \sim 180$ and 250 Å)	74	0.26	24	515	827	3	5	0
4	IC-12-62/1	Pd−0.8, Mn−7.1, La−9.4	$MnLaAl_{11}O_{19}$, $\gamma^{\#}$-Al_2O_3 ($a = 7.937$ Å) PdO ($D \sim 400$ Å)	54	0.29	33	595	829	82	23	0
5	IC-12-62/1	Pd−1.4, Mn−7.1, La−9.4	$MnLaAl_{11}O_{19}$, $LaAlO_3$, α-Al_2O_3 Pd^0 ($D > 500$ Å)	12	0.29	29	700	830	102	40	2
6	IC-12-62/2	Pd−0.8, Mn−5.3, La−9.9	$MnLaAl_{11}O_{19}$, $\gamma^{\#}$-Al_2O_3 ($a = 7.937$ Å), PdO ($D \sim 250$ Å)	45	0.32	30	550	829	7	13	0

The Samples 2, 4 and 5 were prepared using tetrachloropalladic acid, the Samples 3 and 6 were prepared using palladium nitrate; the Samples 1–4 and 6 were calcined at 1273 K, the Sample 5 was calcined at 1373 K. The $\gamma^{\#}$-Al_2O_3 is solid solution based on γ-Al_2O_3 structure.
T_{ign} is ignition temperature of methane–air mixture measured at 5 vol.% CH_4 and 5000 h^{-1}.
T_{in} is inlet temperature of methane–air mixture in experiments in which the CH_4, CO, and NO_x concentrations were measured at the outlet of the catalyst bed with a 300 mm height at 24,000 h^{-1} and $\alpha = 6.6$–6.9.
S_{sp} is specific surface area found by BET method; V_Σ is total pore volume obtained from nitrogen desorption isotherm, P_c is crushing strength of catalyst pellets.

Al_2O_3 (IC-12-62) were synthesized according to the earlier reported procedures [12]. Their physicochemical and catalytic properties are given in Table 1.

2.2. Catalytic activity tests

The catalytic packages were tested in the combustion of natural gas using a CCC of a pilot test installation. The catalytic packages had uniform or combined loading consisting of two or three different catalyst. The catalytic packages are schematically presented in Fig. 1. The total volume of the catalytic package was 1.3 l.

The CCC used for catalytic tests is a stainless-steel tubular vertical reactor with an inner diameter of 76 mm, equipped with four chromel–alumel thermocouples distributed at different positions in catalyst bed (L = 300–340 mm). The CCC was earlier described in [11,12].

The catalyst light-off temperature (T_{ign}) was determined at 5 vol.% CH_4 and GHSV = 5000 h^{-1}.

The air excess coefficient (α) was selected to be close to the minimum value used in the operation of a full-power gas turbine power plant (α = 6.4–6.8). The GHSV was in the range 8500–24,000 h^{-1}. The inlet temperature of the fuel–air mixture T_{in} was varied between 743 and 873 K. After reaching the inlet temperature, the mixture was introduced into the CCC. Due to the methane combustion, the temperature in the catalyst bed increased and was stabilized in 30 min. The temperature at the chamber exit was 1173–1258 K. After stabilization of the catalyst package operation regime CH, CO and NO_x concentrations at the CCC outlet were measured.

2.3. Mathematical modeling

Calculations of the kinetic parameters and the combustion process simulation in the CCC were performed using software developed at the Boreskov Institute of Catalysis.

For the methane oxidation reaction we assumed that only the deep oxidation to CO_2 and H_2O takes place in the oxygen excess. The reaction rate was calculated using Eqs. (1) and (2).

$$W = kC_{CH_4}\left(\frac{P}{P_0}\right) \quad (1)$$

$$k = \eta k_0(1-\varepsilon)\exp\left(-\frac{E/R}{T}\right) \quad (2)$$

where k is the kinetic constant (s^{-1}), C_{CH_4}—the methane concentration (molar fraction), P—the operating pressure (bar), P_0—the pressure (bar) at which the reaction kinetics is studied experimentally (in this case it is equal to 1 bar), η—efficiency factor (dimensionless), k_0—the pre-exponential factor of the kinetic constant (s^{-1}), E—the activation energy (J mol^{-1}), R—the molar gas constant (J mol^{-1} K^{-1}), ε—the void fraction of the catalyst bed (dimensionless).

The values of kinetic parameters (k_0, E) were earlier determined in kinetic experiments on methane oxidation over IC-12-60, IC-12-61 and IC-12-62 catalysts [12]. It was shown that the first-order (with respect to methane concentration) kinetic equation with linear dependence upon pressure provides good description of experimental data in a wide range of methane concentrations and a reasonable range of operation pressures.

The efficiency factor η, accounting for the internal mass transfer limitations, was determined using the standard Thiele equation for the first-order reaction [17].

A heat and mass transfer steady-state model of an ideal displacement adiabatic reactor was used in the simulations of the

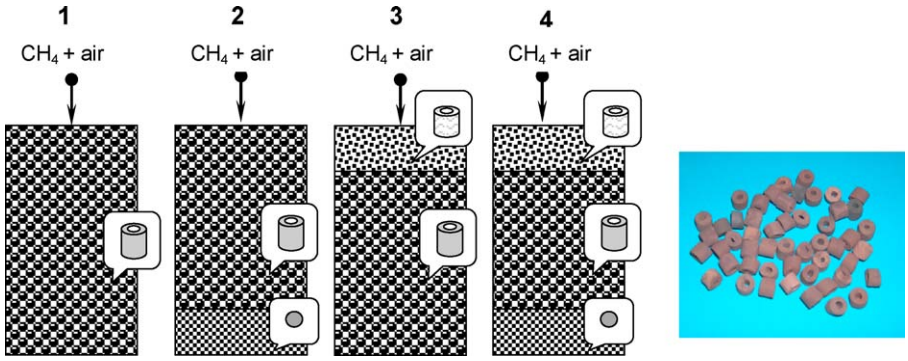

Fig. 1. Modeling of uniform (1) and structured (2–4) loading of the reactor and photo of granulated catalyst.

catalyst bed:

$$u\frac{\partial C_{CH_4}}{\partial \ell} = -W = \beta(C^*_{CH_4} - C_{CH_4}) \quad (3)$$

$$u\frac{\partial T_G}{\partial \ell} = xC^{in}_{CH_4}\Delta T_{ad} = \frac{\alpha}{c_p}(T_C - T_G) \quad (4)$$

$$\ell = 0 \Rightarrow C_i = C_i^{in}; \qquad T = T_{in} \quad (5)$$

where u is the superficial linear gas velocity in the reactor reduced to normal conditions and full reactor sequence ($m\,s^{-1}$), ℓ—the coordinate along the reactor height (m), x—the methane conversion, C^* and C—methane concentrations at the surface of the catalyst grain and in the gas flow respectively (molar fraction), β—the mass transfer coefficient for methane (s^{-1}), T_G and T_C—gas and catalyst temperatures (K) accordingly, ΔT_{ad}—the adiabatic heat rise of the reaction (K), α—the heat transfer coefficient ($W\,m^{-3}\,K^{-1}$), c_p—the gas heat capacity ($J\,m^{-3}\,K^{-1}$), index *in* corresponds to conditions at the reactor inlet.

The mass and heat transfer coefficients were calculated according to the equations presented in [18] with representation of different shapes of catalyst pellets by spheres of equivalent diameter.

3. Results and discussions

3.1. Optimization of catalytic activity and high temperature stability

Earlier, we have developed two types of granulated catalysts for methane combustion in CCC of regenerative low-power gas turbines [12,13]. The first type is Pd catalyst on alumina modified by CeO_2 (commercial trademark IC-12-60). This catalyst initiates the methane ignition at low temperatures, and the combustion products do not contain CO and NO_x (Table 1, Samples 2 and 3). The active component of IC-12-60 catalyst is highly dispersed PdO particles which provides the high activity at low temperatures. The regulation of palladium distribution across the catalyst granule from egg-yolk to uniform and to egg-shell allowed us to decrease the Pd loading to 2 wt.% without loss of the catalyst activity. For example, the two Pd-CeO_2-Al_2O_3 catalysts have been prepared using tetrachloropalladic acid and the palladium nitrate solutions. The former had an egg-yolk Pd distribution with 40 nm Pd particles and initiated the methane oxidation at 573 K (Table 1, IC-12-60/1) [12]. The latter had 20–25 nm Pd particles distributed as an egg-shell, it initiated the methane oxidation at 513 K (Table 1, IC-12-60/2) [12]. Our experimental results correlate with the data of other scientific groups. Palladium catalysts are well known to be most active in deep oxidation of methane and CO [1,3,10,19,20], have a low light-off temperature [1,10], and are stable to thermal sintering in the oxidizing environment [7,21], but the upper temperature limit of their use is about 1073–1173 K [10]. Therefore, we selected our Pd-CeO_2-Al_2O_3 catalysts for initiation of fuel combustion in the upstream section of the combustion chamber.

The second type is the catalysts based on manganese hexaaluminate and manganese hexaaluminate doped by small amounts of Pd (0.5–0.8 wt.%). These catalysts are inexpensive in comparison with the known Pd-Pt catalysts for gas turbines which usually contain 5 wt.% noble metals [3,9,22,23]. The catalyst IC-12-61 containing Mn hexaaluminate is less active in methane oxidation at low temperatures than Pd-CeO_2-Al_2O_3 catalysts (Table 1, Samples 1 and 3), however it exhibits high stability at high temperatures [12]. The doping of the Mn-hexaaluminate catalyst with Pd to 0.8 wt.% from tetrachloropalladic acid (IC-12-62/1) allows a decrease of the ignition temperature by 50 K [15] while retaining high thermal stability of manganese hexaaluminates (Table 1, Sample 4) [14,15]. The use of palladium nitrate (IC-12-62/2) in place of tetrachloropalladic acid as a Pd precursor allows a decrease of the ignition temperature by 90–100 K and a decrease of CO content in the reaction products (Table 1, Sample 6) due to a synergetic effect of Pd and MnO_x on the catalytic activity. The IC-12-62/1 catalyst has PdO particles with a size of 40 nm (coherence area) uniformly distributed in the granule, whereas in the IC-12-62/2 catalyst fine dispersed PdO particles (20–25 nm) are located in the near-surface part of the granule similar to an egg-shell. When the calcination temperature was increased from 1273 to 1373 K, we observed a decrease of the catalytic activity as a result of the specific surface area reduction and transformation of PdO to Pd^0 (Table 1, Sample 5), although the catalyst thermal stability increased due to the completion of manganese hexaaluminate formation. The catalysts IC-12-62/1 and IC-12-62/2 are characterized by high thermal stability at 1173–1373 K and the ability for stable oxidation of lean methane–air mixtures; therefore they can be used in the downstream section of the combustion chamber for high temperature fuel combustion.

Thus, catalysts of these two types can be used for development of a combined catalytic package with a reduced Pd content for small gas turbine power plants. The variation of Pd precursors and modifying additives, Pd loading and calcination temperature exercises control over Pd distribution, Pd particle size and Pd electronic state, and thereby adjusts the catalytic properties and thermal stability, optimizing them to operation conditions of a gas turbine combustor.

3.2. Selection of shape and size of catalyst granules

The ultra-low emission characteristics of CCC are determined not only by the catalyst activity but also by geometric parameters of the catalyst package, such as the bed height and the shape and size of catalyst granules, which are responsible for the efficiency of mass and heat transfer in the fixed catalyst bed. Therefore, the effects of the catalyst granule shape and size on characteristics of the process of catalytic methane combustion: methane conversion,

temperature in the bed and pressure drop were studied. Modeling of the process was performed taking into account the influence of the internal and external diffusion on the kinetic parameters (k_0 and E) for the reaction $CH_4 + 2O_2 \rightarrow CO_2 + 2H_2O$ proceeding on each individual catalyst. The calculations were performed for typical operation conditions of the CCC [11]: methane concentration in methane–air mixture 1.5 vol.%, GHSV = 5000–40,000 h^{-1} and inlet temperature 723–873 K. The model CCC was represented by a tubular reactor with 80 mm inner diameter and 300 mm catalyst bed height.

The methane combustion modeling shows that the shape of the catalyst granules has a substantial effect on methane conversion, and hence on the residual methane content and the temperature in the catalyst bed. This effect increases with a decrease of the inlet temperature and an increase of the space velocity, being most marked for catalysts with lower activity. Fig. 2 shows simulated profiles of the residual methane content upon methane oxidation in uniform beds of the IC-12-61 catalysts with different shape: ring (7.5 mm × 7.5 mm × 2.5 mm), cylinder (4.5 mm × 5.0 mm) and sphere (5.0 mm). At 723 K and 10,000 h^{-1}, the residual methane contents attained in the beds of spherical and ring-shaped granules of IC-12-61 catalyst are different by a factor of 4.5, but neither of the catalyst shapes provides the required methane emission level (not exceeding 10 ppm) at GHSV higher than 5000 h^{-1}. At higher GHSV, the required methane residual concentration is attained only at the increase of the inlet temperature with a similar effect of the granule shape. For instance, at GHSV below 20,000 h^{-1} the residual methane content less than 10 ppm is observed at the inlet temperature of 823 K for the beds of both ring-shaped and spherical granules, while at 35,000 h^{-1} this methane concentration is attained only on the spherical granules and at a higher temperature of 873 K.

According to modeling, the methane conversion increases with the change of granule shape in the sequence: ring < cylinder < sphere. However, the use of cylindrical and spherical catalyst for the entire reactor is impossible due to a high pressure drop (Fig. 2B). As shown in Fig. 2B, catalytic packages with a height of 300 mm containing ring-shaped and spherical granules give the pressure loss of up to 0.5 and 1.2 bar, respectively.

Thus, in the loading of the CCC with granulated catalysts, the attention should be paid not only to the ultra-low emission characteristics, but also to the minimization of the pressure drop in the catalyst bed. The structured combined catalytic package containing two or three catalysts with optimal catalytic properties and geometrical parameters seems to be promising to meet these two requirements. In design of a combined catalytic package with a

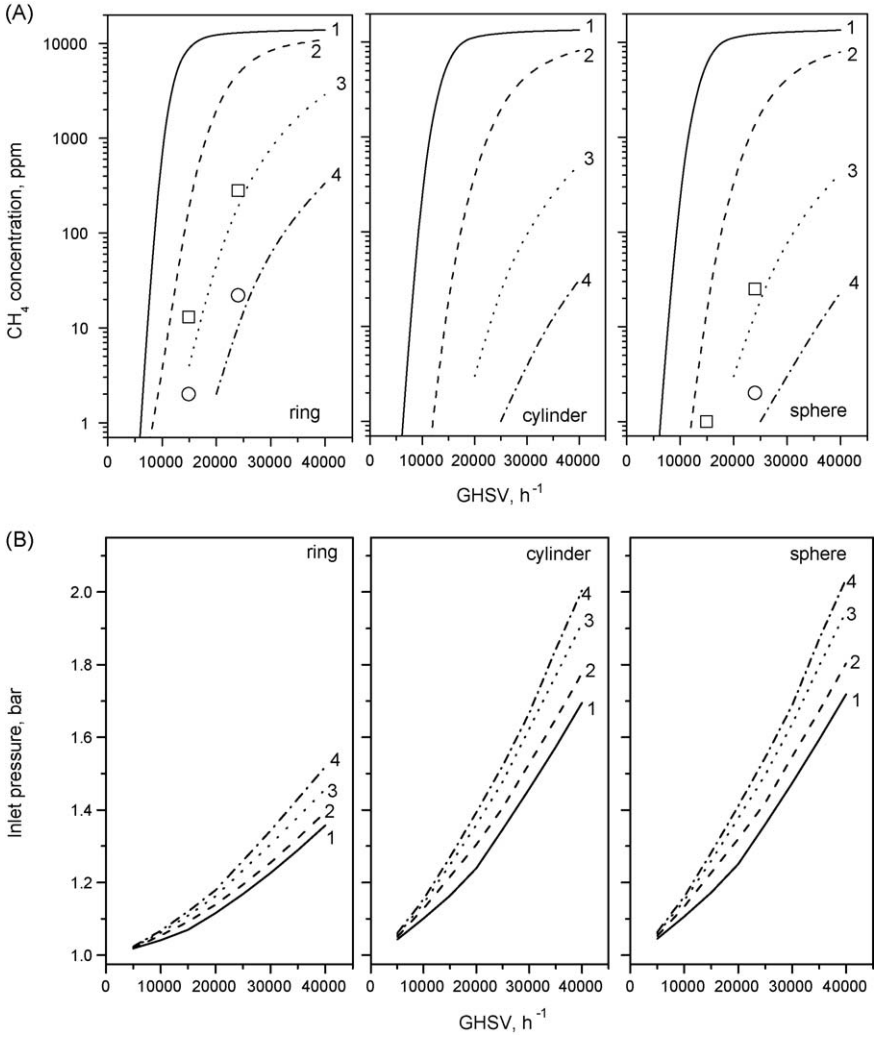

Fig. 2. Simulated profiles of residual methane concentration (A) and inlet pressures (B) vs. GHSV at temperatures: 723 K (Curve 1), 773 K (Curve 2), 823 K (Curve 3) and 873 K (Curve 4) for uniform catalyst package loaded with Mn-La-Al_2O_3 catalyst (IC-12-61) as ring, spherical, and cylindrical granules with size 7.5 mm × 7.5 mm × 2.5 mm, 5.0 mm, and 4.5 mm × 5 mm, respectively. The CCC diameter is 80 mm and the height is 300 mm. Methane concentration is 1.5 vol.%, α = 6.9. Experimental data are presented for comparison: 773 K (□) and 873 K (○).

high efficiency and a long lifetime, first of all, the light-off temperature and the operation temperature limit of the catalysts should be taken into account, because the CCC having a low light-off temperature of lean methane–air mixtures and high thermal stability provides stable combustion of methane–air mixtures and low emission characteristics. It should be noted that at high inlet temperatures and high methane concentrations the maximum temperature in the catalyst bed can be as high as 1373–1473 K, which can result in the reduction of the catalyst lifetime. Further, three types of catalyst packages complying with the above requirements are examined.

3.3. Variation of the structure of combined catalyst loading in the CCC

3.3.1. Two high temperature catalysts with different granule shapes

The reactor consists of two sections: the first one with the ring shaped oxide catalyst Mn-La-Al_2O_3 or this catalyst modified by Pd (0.5–0.8 wt.%), and the second downstream section with the spherical catalyst having lower fractional void volume. This combination with a shorter bed of spherical catalyst (about 20%) provides rather high methane combustion efficiency at a minor increase of pressure drop (not exceeding 20%) in comparison with the uniform catalytic package. For example, at 40,000 h^{-1} and 873 K, the residual CH_4 content decreased twice and the pressure drop increased only by 18%, when 20% of the ring-shaped Mn-La-Al_2O_3 catalyst was replaced by the spherical granules (Figs. 2A and 3A).

The simulation of methane combustion process shows that the catalytic package with Pd-Mn-La-Al_2O_3 (Fig. 3B) is more effective than the one with Mn-La-Al_2O_3 (Fig. 3A). At similar conditions, the former provides the residual methane concentration 10 times lower than the latter, methane content being below 10 ppm at 25,000 h^{-1} and a temperature as low as 773 K. This catalytic package has also high efficiency at 40,000 h^{-1}, although at a higher inlet temperature (873 K). The catalytic packages with both Pd-Mn-La-Al_2O_3 and Mn-La-Al_2O_3 have a similar thermal stability at temperatures up to 1373 K.

3.3.2. Two ring shaped catalysts with different catalytic activity

In this case, a short ignition bed (ca. 10%) of the highly active Pd catalyst is located in the upstream section with a lower temperature. The larger bed of high temperature tolerant Mn-La-Al_2O_3 or Pd-Mn-La-Al_2O_3 catalyst in the downstream section provides practically total methane combustion. This design of the catalyst package allows a reduction of the total Pd loading and an increase of methane combustion efficiency at low inlet temperatures.

Modeling of methane combustion process shows that the use of Pd-CeO_2-Al_2O_3 catalyst is more preferable; however the catalyst package formed from Pd-Mn-La-Al_2O_3 is also rather efficient. The location of a more active catalyst in the upstream section is more advantageous in comparison with a variant of its downstream location (Fig. 4). For example, at the same conditions of 40,000 h^{-1} and 873 K, the simulated residual methane content achieved over the former package does not exceed 10 ppm, while with the latter it is as high as 125 ppm. The effect of the variation of the length of the two sections and space velocity on the process parameters was also studied and showed that the optimal loading of highly active Pd catalyst is close to 10% of the total catalyst loading of the CCC.

3.3.3. Three catalysts with different catalytic activity and fractional void volume

The highly active Pd catalyst in the upstream section initiates methane oxidation, the high temperature tolerant catalyst in the larger middle section provides stable methane combustion. The bicomponent Pd-Mn-La-Al_2O_3 catalyst with a low Pd content and low fractional void volume in the downstream section improves the efficiency by removal of methane residual traces.

The modeling showed that the substitution of 10% of Mn-La-Al_2O_3 catalyst (Fig. 3A) for Pd-CeO_2-Al_2O_3 in the upstream section and the introduction of spherical Pd-Mn-La-Al_2O_3 catalyst in the downstream section of the catalytic package (Fig. 4C) allow a decrease of the inlet temperature and an increase of GHSV. For example, at 20,000 h^{-1} the inlet temperature can be reduced from 873 to 723 K. For the package operation at a higher GHSV (30,000 h^{-1}), an increase of the inlet temperature to 773 K is required. It should be noted that the cost of the combined catalyst package is not significantly higher than that of the uniform Mn-La-Al_2O_3 catalyst bed.

3.4. Comparison of simulated and experimental data

Experimental runs with a model reactor (1.3 l catalyst) demonstrated very good correlation with the results of the

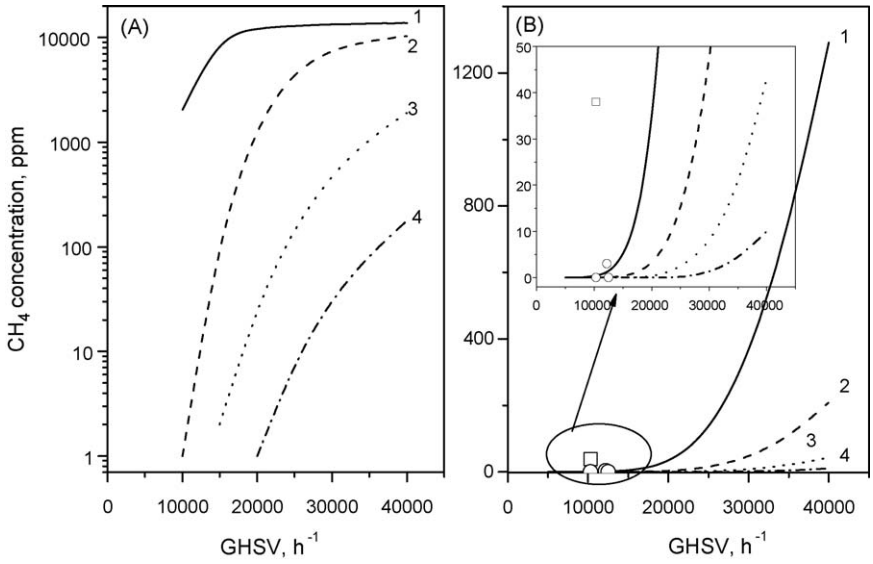

Fig. 3. Simulated profiles of residual methane concentration vs. GHSV at temperatures: 723 K (Curve 1), 773 K (Curve 2), 823 K (Curve 3) and 873 K (Curve 4) for combined catalyst package loaded with Mn-La-Al_2O_3 (A) and Pd-Mn-La-Al_2O_3 (B) catalysts in accordance with Scheme 2 {ring (7.5 mm × 7.5 mm × 2.5 mm), L = 280 mm} + {sphere (5.0 mm), L = 60 mm}. Methane concentration is 1.5 vol.%, α = 6.9. Experimental data are presented for comparison: 743 K (□) and 853 K (○).

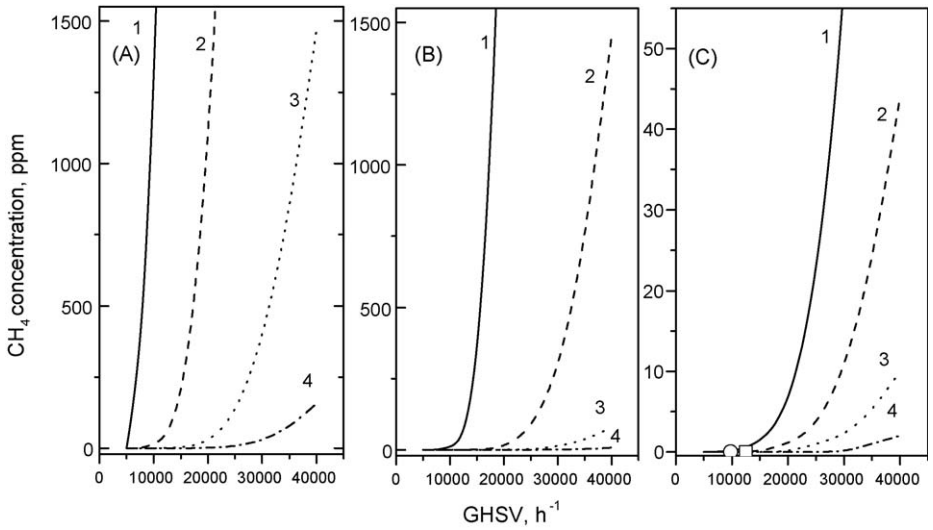

Fig. 4. Simulated profiles of residual methane concentration vs. GHSV at temperatures: 723 K (Curve 1), 773 K (Curve 2), 823 K (Curve 3) and 873 K (Curve 4) for combined catalyst packages in accordance with Scheme 3 (A and B) and Scheme 4 (C). Methane concentration is 1.5 vol.%, α = 6.9. Experimental data are presented for comparison: 743 K (□) and 853 K (○). (A) Mn-La-Al_2O_3 {ring 7.5 mm × 7.5 mm × 2.5 mm, L = 260 mm} + Pd-Mn-La-Al_2O_3 {ring 7.5 mm × 7.5 mm × 2.5 mm, L = 40 mm}, (B) Pd-Mn-La-Al_2O_3 {ring 7.5 mm × 7.5 mm × 2.5 mm, L = 260 mm} + Mn-La-Al_2O_3 {ring 7.5 mm × 7.5 mm × 2.5 mm, L = 40 mm}, (C) Pd-CeO_2-Al_2O_3 {ring 7.5 mm × 7.5 mm × 2.5 mm, L = 40 mm} + Mn-La-Al_2O_3 {ring 7.5 mm × 7.5 mm × 2.5 mm, L = 240 mm} + Pd-Mn-La-Al_2O_3 {sphere 5.0 mm, L = 60 mm}.

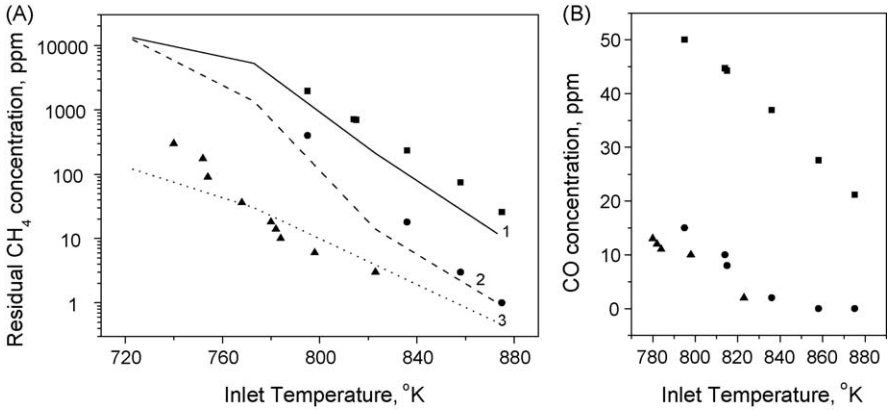

Fig. 5. Residual methane concentration (A) and CO concentration (B) vs. inlet temperature of CCC at GHSV = 24,000 h^{-1} and α = 6.8. Uniform catalyst package loaded with Mn-La-Al_2O_3 catalyst (IC-12-61) as rings (■, Curve 1) and spheres (●, Curve 2), having size 7.5 mm × 7.5 mm × 2.5 mm and 5 mm, respectively, and Pd-Mn-La-Al_2O_3 catalyst (IC-12-62/2) as rings (▲, Curve 3) with size 7.5 mm × 7.5 mm × 2.5 mm. The symbols are experimental data, the lines are calculated data.

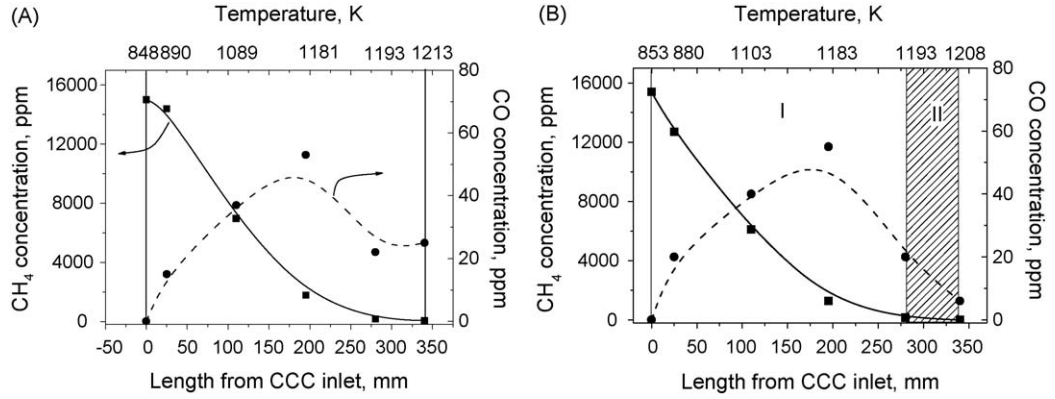

Fig. 6. Profiles of methane (■) and CO (●) concentrations and temperatures along the CCC length during combustion of natural gas in a combined catalyst package: (A) Scheme 1: Pd-Mn-La-Al_2O_3 (ring, 340 mm) at T_{in} = 575 °C, GHSV = 15,000 h^{-1}, α = 6.8; (B) Scheme 2: Pd-Mn-La-Al_2O_3 (ring, 280 mm)/Pd-Mn-La-Al_2O_3 (sphere, 60 mm) at T_{in} = 580 °C, GHSV = 15,000 h^{-1}, α = 6.9.

modeling (Figs. 2A, 3B and 4C). The catalytic package with the spherical or ring-shaped granules of the IC-12-61 catalyst provided methane combustion to 1 ppm and 15 ppm residual methane concentration, respectively, in the pilot test installation at 15,000 h^{-1} and 773 K and to 2 ppm at 24,000 h^{-1} and 873 K (Fig. 2).

Fig. 5 shows the correlation between the simulated and experimental data for the residual methane concentrations in a uniform catalytic package with the ring-shaped Mn-La-Al_2O_3 and Pd-Mn-La-Al_2O_3 catalysts at 24,000 h^{-1} as a function of the inlet temperature. The observed deviation of the experimental data on residual methane content from the simulated curves can be explained by two causes. The excess of the experimental values over the simulated ones can be caused by the heat loss. Lower experimental values of the residual methane content in comparison with the calculated ones for the catalyst Pd-Mn-La-Al_2O_3 in the range of the inlet temperatures 773–823 K are probably due to the contribution of other heterogeneous reactions (different from deep oxidation) and gas-phase homogeneous methane oxidation. The carbon dioxide reforming and the partial methane oxidation as well as gas phase reactions have not been incorporated into our simulation yet, because we have not observed CO and H_2 formation in the kinetic experiments [12]. Noticeable amount of CO (10–14 ppm, Fig. 5 B) was observed in the pilot test installation when the CCC was loaded by ring-shaped and/or spherical catalyst granules with a size 7.5 mm × 7.5 mm × 2.5 mm and 5 mm, respectively. Carbon monoxide can be formed as an intermediate product of homogeneous methane oxidation, which has been shown in the study of methane oxidation in lean mixtures at 900–1400 K [5]. Our assumption about the contribution of gas phase methane oxidation agrees with a decrease of the CO concentration when the ring-shaped granules are totally (Fig. 5B) or partially substituted (Fig. 6B) for spherical granules. The ring-shaped and spherical granules are different by the specific external surface (593 and 693 m^{-1}, respectively) and the void fraction in the catalyst bed (ε = 0.5 and 0.42, respectively). It is well known that the increase of the surface and the reduction of the void fraction lead to an increase of free radical decay.

On the other hand, there is strong evidence that the catalyst surface affects the gas-phase chemistry [24–28]. The hexaaluminate catalyst surface is assumed to act as a sink for methyl radicals, suppressing gas-phase reactions [24]. The authors of [24] made this assumption from comparison of the experimental data with numerical models that include both surface and gas phase chemistry. We also observed that the CO concentration changes along the catalyst bed increasing with the temperature increase up to 1173 K but decreasing at the further rise of the temperature (Fig. 6). The arched profile of the formed CO can be evidence that CO is the intermediate in the multi-step surface reactions mechanism proposed by Deutschmann and coworkers [25,28], Chou et al. [26] and Aghalayam [27] for the oxidation of lean methane–air mixtures.

4. Conclusions

Modeling of methane combustion in several types of catalyst packages composed of 2 or 3 beds of granulated catalysts different by chemical composition and the shape and/or the size of granules has been performed. It has been shown that the high efficiency of methane combustion (>99.97%) and low emission of HC < 10 ppm can be achieved for all models of catalytic package at variation of the inlet temperature.

The highly active Pd-CeO_2-Al_2O_3 and Pd-Mn-La-Al_2O_3 catalysts should be used in the CCC upstream section for the initiation of methane oxidation. The Mn-La-Al_2O_3 and Pd-Mn-La-Al_2O_3 catalysts with hexaaluminate structure exhibiting good high-temperature activity and high thermal stability can be recommended for the stable methane combustion at a high combustion efficiency in the CCC downstream section. The replacement of 20% of the ring-shaped Mn-La-Al_2O_3 catalyst by the spherical low-percentage Pd-hexaaluminate catalyst in the exit part of the CCC downstream section results in improvement of methane combustion efficiency at a minor increase of the pressure drop (not exceeding 20%). The addition of 10% of the highly active Pd-CeO_2-Al_2O_3 and Pd-Mn-La-Al_2O_3 catalysts with ring shape in the CCC upstream section of such catalytic package provides the required emission characteristics (CH < 10 ppm) at the low inlet temperature (about 723 K) and the high GHSV of lean methane–air mixtures (>20,000 h^{-1}). Experimental runs in the pilot reactor (1.3 kg catalyst) demonstrated very good correlation with the results of the modeling.

Acknowledgment

This study was supported by Integration projects of RAS Presidium 7.2, 7.4 and 19; RFBR (Grants 06-08-00981 and 07-08-12272) and State Contract 02.526.12.6003.

References

[1] D.L. Trimm, Appl. Catal. 7 (1983) 249.
[2] W.C. Pfefferle, J. Energy 2 (1978) 142.
[3] R.A. Dalla Betta, J.C. Schlatter, D.K. Yee, D.G. Loffler, T. Shoji, Catal. Today 26 (1995) 329.
[4] Z.R. Ismagilov, M.A. Kerzhentsev, Catal. Today 47 (1999) 339.
[5] M. Reinke, J. Mantzaras, R. Bombach, S. Schenker, A. Inauen, Combust. Flame 141 (2005) 448.
[6] R.A. Dalla Betta, T. Rostrup-Nielsen, Catal. Today 47 (1999) 369.
[7] J.G. McCarty, M. Gusman, D.M. Lowe, D.L. Hildenbrand, K.N. Lau, Catal. Today 47 (1999) 5.
[8] R. Garroni, T. Griffin, J. Mantzaras, M. Reinke, Catal. Today 83 (2003) 157.
[9] J.G. McCarty, V. Wong, Catalytic Combustion Process, US 6,015,285 (2000).
[10] R.J. Farrauto, M.C. Hobson, T. Kennelly, E.M. Waterman, Appl. Catal. A 81 (1992) 227.
[11] V.N. Parmon, Z.R. Ismagilov, O.N. Favorski, A.A. Belokon, V.M. Zakharov, Herald Russ. Acad. Sci. 77 (2007) 819.
[12] Z.R. Ismagilov, N.V. Shikina, S.A. Yashnik, A.N. Zagoruiko, S.R. Khairulin, M.A. Kerzhentsev, V.N. Korotkikh, V.N. Parmon, B.I. BBraynin, V.M. Zakharov, O.N. Favorski, Kinet. Catal. 49 (6) (2008) 873.
[13] Z.R. Ismagilov, N.V. Shikina, S.A. Yashnik, A.N. Zagoruiko, M.A. Kerzhentsev, V.A. Ushakov, V.A. Sazonov, V.N. Parmon, V.M. Zakharov, B.I. Braynin, O.N. Favorski, Catal. Today, submitted for publication.
[14] L.T. Tsykoza, S.A. Yashnik, Z.R. Ismagilov, R.A. Shkrabina, N.A. Korjabkina, V.V. Kuznetsov. Catalyst for high-temperature combustion of hydrocarbon fuels. Russian Patent RU 2185238 (2002).
[15] S.A. Yashnik, Z.R. Ismagilov, V.V. Kuznetsov, V.V. Ushakov, V.A. Rogov, I.A. Ovsyannikova, Catal. Today 117 (2006) 525.
[16] Z.R. Ismagilov, M.A. Kerzhentsev, V.A. Sazonov, L.T. Tsykoza, N.V. Shikina, V.V. Kuznetsov, V.A. Ushakov, S.V. Mishanin, N.G. Kozhukhar, G. Russo, O. Deutschmann, Kor. J. Chem. Eng. 20 (2003) 461.
[17] O.A. Malinovskaya, V.S. Beskov, M.G. Slin'ko, Modelling of the Catalytic Processes on the Porous Pellets, Novosibirsk, Nauka, 1975.
[18] M.E. Aerov, O.M. Todes, D.A. Narinski, Apparatuses for Steady-State Granular Bed. Hydraulic and Thermal Operation Basics, Khimiya, Leningrad, 1979 (in Russian).
[19] R. Burch, M.J. Hayes, J. Mol. Catal. A 100 (1995) 13.
[20] J.H. Lee, D.L. Trimm, Fuel Process. Technol. 42 (1995) 339.
[21] J.J. Spivey, J.B. Butt, Catal. Today 11 (1992) 465.
[22] A. Ersson, H. Kušar, R. Carroni, T. Griffin, S. Jaras, Catal. Today 83 (2003) 265.
[23] K. Persson, A. Ersson, A. Manrique Carrera, J. Jayasuriya, R. Fakhrai, T. Fransson, S. Jaras, Catal. Today 100 (2005) 479.
[24] R.W. Sidwell, H. Zhu, R.J. Kee, D.T. Wickham, Combust. Flame 134 (2003) 55.
[25] O. Deutschmann, L.I. Maier, U. Riedel, A.H. Stroemman, R.W. Dibble, Catal. Today 59 (2000) 141.
[26] C.P. Chou, J.Y. Chen, G.H. Evans, W.S. Winters, Combust. Sci. Technol. 150 (1) (2000) 27.
[27] P. Aghalayam, Y.K. Park, N. Fernandes, V. Papavassiliou, A.B. Mhadeshwar, D.G. Vlachos, J. Catal. 213 (1) (2003) 23.
[28] R.R. Quiceno, J. Perez Ramirez, J. Warnatz, O. Deutschmann, Appl. Catal. A: Gen. 303 (2000) 166.